Research Article Vol. 29, No. 24 / 22 Nov 2021 / Optics Express 39709

Optics EXPRESS

Extended axial irradiances: Barker rings

CRISTINA M. GÓMEZ-SARABIA,[1] ANGEL SAUCEDA-CARVAJAL,[1] LUIS M. LEDESMA-CARRILLO,[2,3] MIGUEL TORRES-CISNEROS,[4] AND JORGE OJEDA-CASTAÑEDA[4,*]

[1] Departamento de Artes Digitales y Gestión Empresarial, DICIS, University of Guanajuato, Salamanca 36885, Mexico
[2] Instituto de Ingeniería y Tecnología de la Universidad Autónoma de Ciudad Juárez, Mexico
[3] Estudios Multidisciplinarios, University of Guanajuato, Yuriria 38940, Mexico
[4] Electronics Department, DICIS, University of Guanajuato, Salamanca 36885, Mexico
[*] jojedacas@ugto.mx

Abstract: For extending focal depth we employ a set of transparent concentric rings, which are coded with the Barker sequences of length L. At the neighborhood of the paraxial focal plane, these transparent masks generate an axial uniform distribution, which is modulated with sinusoidal variations. For imaging applications, one can extend focal depth if the Barker length is congruent to unity modulo 4. And, for optical trapping, a bottle neck irradiance distribution is generated if the Barker length is congruent to three modulo 4.

1. Introduction

For several optical applications, it is convenient to introduce nonconventional modulations at the pupil aperture of an optical system. Among other applications, we notice the use of the Hadamard matrices for increasing the light gathering power of optical spectrometers [1,2]. For imaging applications, it is convenient to employ masks that are coded with Walsh sequences [3–8]. And now, it is known that one can control the depth of field of an optical system, without reducing the pupil aperture, by employing suitable, tunable phase variations [9–11].

For non-imaging applications, we note the use of angularly coded phase masks, which are used for generating an extended dark spot along the optical axis [12–14]. For detecting in-plane rotations, it is convenient to exploit the autocorrelation properties of angularly coded masks [15]. Relevant to our current discussion, we note that there are several proposals for extending the focal depth of an optical system, without reducing the light gathering power [16–19].

Here, we describe a nonconventional method for increasing focal depth while preserving high light throughput. To this end, we use of a set of transparent concentric disks, which are radially coded with the Barker sequences [20,21]. These phase-only disks are radially distributed as in a zone plate.

In what follows we show that, at the neighborhood of the Gaussian focal plane, one can generate axially extended irradiance distributions. For imaging applications, we recognize the following. At the paraxial focal plane, the increased axial irradiance distribution has a maximum value, if the set of disks are coded with the Barker sequence of either length L = 5 or of length L = 13.

Furthermore, for applications related to particle confinement, we identify a different property. At the neighborhood of the Gaussian focal plane, the increased axial irradiance distributions can have a minimum value, at the paraxial focal plane. For achieving this later result, the proposed set of concentric disks should be coded with the Barker sequences with length equal to L = 3, or L = 7, as well as with L = 11. By using modular arithmetic arguments [21], we note that for the first set of concentric disks, the lengths are congruent to unity modulo four. And, for the second set of concentric disks, the lengths are congruent to three modulus four.

#438772 https://doi.org/10.1364/OE.438772
Journal © 2021 Received 28 Jul 2021; revised 21 Oct 2021; accepted 4 Nov 2021; published 15 Nov 2021

Optics EXPRESS

For the sake of completeness of our proposal, in section 2, we briefly describe the Barker sequences. In section 3, we discuss the use of a set of L concentric disks, which are radially distributed as in a zone plate. In section 4, we apply the autocorrelation properties of the Barker sequence for reporting formula that describe the novel axial irradiance distributions. And in section 5, we summarize our contribution.

2. Optical coding using the Barker sequences

The Barker sequences are a set of L binary numbers. The integer number L is denoted as the length of the sequence. For assuring that the sequences have a middle element, here, we consider lengths that are expressed as odd integer number, $L = 2N + 1$. This feature is noted along both, the first column and the second column of Table 1. Consequently, under our current discussion, a Barker sequence reads $B(N) = \{B_{-N}, \ldots, B_0, \ldots B_N\}$. In Table 1, along the fourth column, we list five sequences that are relevant to our current task.

Table 1. Main features of the Barker sequences of length $L = 2n + 1$.

N	L = 2 N + 1	Mod $_4$ (L)	B(N)	Secondary Correlation Lobes
1	3	3	{1,1, -1}	-1
2	5	1	{1,1,1-1,1}	1
3	7	3	{1,1,1, -1, -1,1, -1}	-1
5	11	3	{1,1,1, -1, -1, -1,1, -1, -1,1, -1}	-1
6	13	1	{1,1,1,1,1, -1, -1,1,1, -1,1, -1,1}	1

The Barker sequences are employed in RADAR engineering for achieving highly peaked autocorrelation on the main lobe. There are several side-lobes that have reduced values. The side-lobes can be either equal to unity or equal to minus unity as depicted in Fig. 1. In section 4, we apply this autocorrelation property for reporting novel formulas, which describe nonconventional axial irradiance distributions.

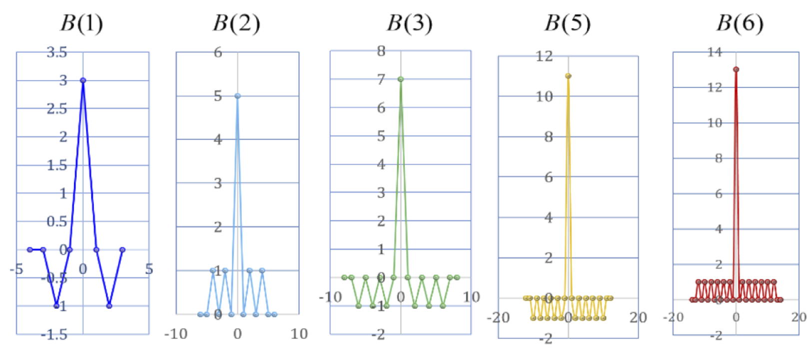

Fig. 1. Autocorrelations of the Barker sequences of length $L = 2N + 1$. The side-lobes have positive values if $N = 2$ and $N = 6$. And they have negative values if $N = 1$, $N = 3$, and $N = 5$. In these plots, both axes are in arbitrary dimensionless units.

In Fig. 2 we depict a classical optical processor that employs, as a spatial filter, a set of L concentric disks. In this optical setup, the two depicted lenses have a focal length that is equal to f. The back focal plane of the second lens is here denoted as the paraxial focal plane of the optical system. The location of this plane is specified with the value $z = 0$. Along the z-axis, the irradiance distributions are denoted as the axial irradiance distributions.

At the Fraunhofer plane, the radius of the circular pupil aperture is r, and its maximum value is h. The wavelength is denoted as λ. In this plane, we use polar coordinates $(\rho = r / (\lambda f), \varphi)$.

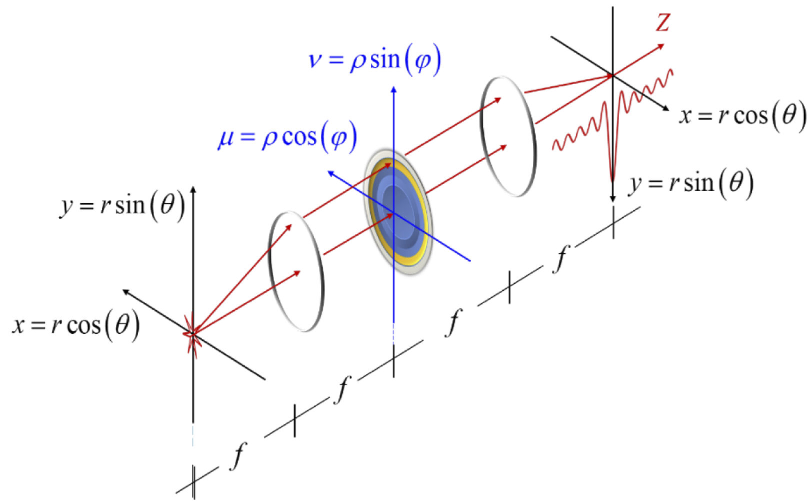

Fig. 2. Optical setup depicting the use of a set of L concentric, transparent rings that are located at the Fraunhofer plane of the optical processor. At the image plane, the focal plane of the final lens, the axial coordinate z is equal to zero.

The lower-case Greek letter ρ denotes a radial spatial frequency, whose maximum value is the cutoff spatial frequency Ω. Equivalently, the cut-off spatial frequency is equal to $\Omega = h / (\lambda f)$. The lower-case Greek letter φ is the polar angle. At the image space, we employ cylindrical coordinates (r, θ, z).

Under the paraxial regime, at the image space [22,23], the complex amplitude distribution is

$$p(r,\theta,z) = \int_0^{\Omega}\int_0^{2\pi} P(\rho)\ \exp(-i\pi\lambda z\rho^2)\ \exp(i2\pi r\rho\cos(\theta-\varphi))\rho\, d\rho\, d\varphi. \tag{1}$$

In Eq. (1) we denote the complex amplitude transmittance of the radially symmetric pupil as P(ρ). By setting $r = 0$, in Eq. (1), one obtains that the axial complex amplitude distribution is

$$p(0,\theta,z) = 2\pi\int_0^{\Omega} P(\rho)\ \exp(-i\pi\lambda z\rho^2)\ \rho\, d\rho. \tag{2}$$

Now, it is convenient to employ the following geometrical transformation

$$\zeta = \left(\frac{\rho}{\Omega}\right)^2 - \frac{1}{2};\quad P(\rho)\ circ\left(\frac{\rho}{\Omega}\right) = Q(\zeta)\ rect(\zeta). \tag{3}$$

In Eq. (3) the lower-case Greek letter ζ denotes a dimensionless variable that helps to transform a rectangular aperture into a circular aperture. Now, for relating our results with the classical treatment of wave aberrations, we employ the following change of variable

$$W = -\left(\frac{\lambda^2\Omega^2}{2}\right) z;\quad q(W) = p(0,\theta,z). \tag{4}$$

The change of variable in Eq. (4) helps to transform the quadratic phase factor, inside the integrand of Eq. (2), into the following linear phase factor

$$\exp[-i\pi\lambda z\rho^2] = \exp\left[i\pi\left(\frac{W}{\lambda}\right) + i2\pi\left(\frac{W}{\lambda}\right)\zeta\right]. \tag{5}$$

Optics EXPRESS

In Fig. 3 we illustrate the above geometrical transformations, which are useful for relating 1-D complex amplitude transmittances, Q(ζ), with 2-D complex amplitude transmittances that have only radial variations, P(ρ).

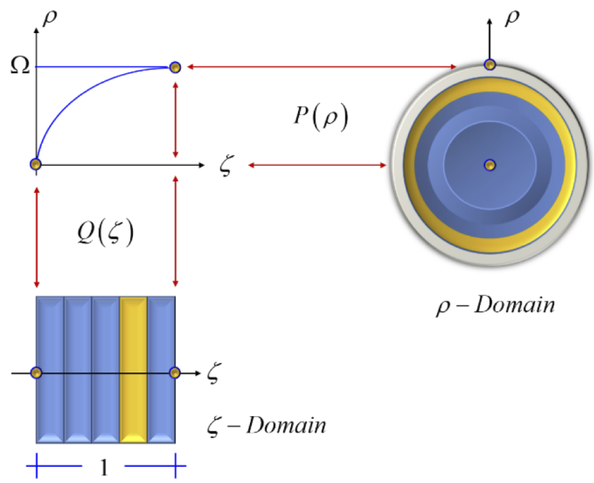

Fig. 3. Pictorial of the geometrical transformation that is useful for changing 2-D radial variations into the 1-D rectangular variations. In this pictorial, the Barker sequence has a length equal to five. The blue regions represent amplitude transmittance equal to unity, while the orange regions represent amplitude transmittance equal to minus unity.

If in Eq. (2) one substitutes the new variables, in Eq. (3), the axial complex amplitude distribution reads

$$q(W) = 2\pi \exp\left(i\pi\frac{W}{\lambda}\right) \int_{\zeta=-0.5}^{0.5} Q(\zeta)\, \exp\left[i\,2\pi\left(\frac{W}{\lambda}\right)\zeta\right]\, d\zeta. \tag{6}$$

In the following section we use Eq. (6) for describing the use of phase-only masks that are coded with the Braker sequences.

3. Barker disks

Now, for employing the Barker sequences as codes, we divide a 1-D, rectangular pupil aperture into (2 N +1) sub apertures, rectangular windows. At each sub aperture, the complex amplitude transmittance is equal to the value of an element in the Barker sequence, with length L = 2 N +1. In mathematical terms, the 1-D pupil aperture has the following complex amplitude transmittance

$$Q_{2N+1}(\zeta) = \sum_{n=-N}^{N} B_n(N)\; rect\left(\frac{\zeta-\zeta_n}{\Delta\zeta}\right). \tag{7}$$

In Eq. (7) at each rectangular sub aperture is represented by a rectangular function. Its width is equal to Δζ, and its middle point is located at the positions ζ_n. In mathematical terms,

$$\Delta\zeta = \frac{1}{(2N+1)}; \quad \zeta_n = \frac{n}{(2N+1)}. \tag{8}$$

Due to the geometrical transformation in Eq. (3), in the radial domain the equivalent expressions are as follows. The radial complex amplitude transmittance is

$$P_{2N+1}(\rho) = \sum_{n=-N}^{N} B_n(N)\; circ\left(\frac{\rho-\rho_n}{\Delta\rho_n}\right). \tag{9}$$

Optics EXPRESS

The centers of the rings are at the radial positions ρ_n, and the width of the rings are $\Delta\rho$. Their explicit expressions are, respectively,

$$\begin{aligned} \rho_n &= \Omega\sqrt{\left(\frac{2N+2n+1}{2(2N+1)}\right)}; \\ \Delta\rho_n &= \Omega\left[\sqrt{\left(\frac{N+n+1}{2N+1}\right)} - \sqrt{\left(\frac{2N+2n+1}{2(2N+1)}\right)}\right]. \end{aligned} \tag{10}$$

In Fig. 4 we show pictorials of the rectangular windows, as well as pictorials of their associated rings. If the region is depicted in blue, then the amplitude transmittance is equal to unity. And if the amplitude transmittance is equal to minus unity, then the region is depicted in orange.

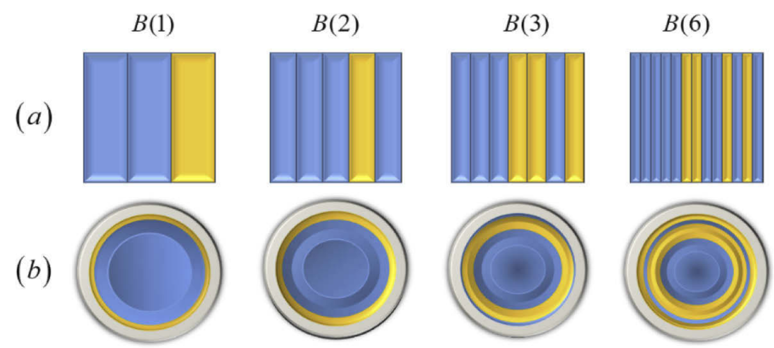

Fig. 4. Pictorial of the regions that are coded with the Braker sequences. The blue regions represent amplitude transmittance equal to unity, while the orange regions represent amplitude transmittance equal to minus unity. In (a) the rectangular windows in the ζ-domain. In (b) the rings in the ρ-domain.

Next, we evaluate the axial irradiance distributions that are generated by using the proposed phase-only rings.

4. Autocorrelation shaped irradiances

If one substitutes Eq. (8) in Eq. (7), and after taking the squared modulus, one obtains that the axial irradiance distribution, which reads

$$|q_{2N+1}(W)|^2 = \left|\sum_{n=-N}^{N} B_n(N)\exp\left[i\,2\,\pi\left(\frac{n}{\lambda(2N+1)}\right)W\right]\right|^2 \operatorname{sinc}^2\left[\left(\frac{W}{\lambda(2N+1)}\right)\right]. \tag{11}$$

From the last term in Eq. (11), it is apparent that the axial irradiance distribution has an envelope, which is equal to a sinc function to the square power. This envelope has a width that increases as the factor $(2\,N+1)$ increases. Trivially, since for the clear pupil aperture $N=1$, the result in Eq. (11) implies that the finite size of the rings helps to spread the axial irradiance envelope.

Next, for making a proper assessment of the first term in Eq. (9), it is convenient to employ the definition of the Strehl ratio versus focus errors. The definition reads

$$S_{2N+1}(W) \triangleq \frac{|q_{2N+1}(W)|^2}{|q_{2N+1}(0)|^2}. \tag{12}$$

By substituting Eq. (9) in Eq. (10), one obtains an analytical expression for the Strehl ratio versus focus errors, associated to the Barker disks; namely

$$S_{2N+1}(W) = \frac{\left| \sum_{n=-N}^{N} B_n(N) \exp\left[i\, 2\,\pi \left(\frac{n}{\lambda(2N+1)} \right) W \right] \right|^2}{\left| \sum_{n=-N}^{N} B_n(N) \right|^2} \operatorname{sinc}^2\left[\left(\frac{W}{\lambda(2N+1)} \right) \right]. \tag{13}$$

Now, it is convenient to take advantage of the correlation properties of the Barker sequences, by rewriting Eq. (11) as

$$S_{2N+1}(W) = \frac{(2N+1) + 2 \sum_{m=1}^{2N} \left[\sum_{n=-N}^{N-|m|} B_{|m|+n}(N)\, B_n(N) \right] \cos\left[2\,\pi \left(\frac{m}{(2N+1)\lambda} \right) W \right]}{(2N+1) + 2 \sum_{m=1}^{2N} \left[\sum_{n=-N}^{N-|m|} B_{|m|+n}(N)\, B_n(N) \right]} \operatorname{sinc}^2\left[\left(\frac{W}{\lambda(2N+1)} \right) \right]. \tag{14}$$

It is clear from Eq. (12) that inside the axial irradiance envelope, there are axial irradiance variations that are composed by two terms. There is a uniform background that is equal to the length of the Barker sequence, $L = 2\,N + 1$. And there is a weighted sum of sinusoidal variations, whose modulations are equal to the autocorrelation function of the Barker sequence.

In Fig. 5, we plot the axial irradiance distributions depicting these features. For further discussing their characteristics, as a reference, we have plotted a black dotted curve. This dotted curve describes the axial irradiance distribution associated to a clear pupil aperture, that is $\operatorname{sinc}^2(W/\lambda)$. From a simple visual comparison between the dotted curve and the full line curves, we claim that the propose mask are able to extend the axial irradiance distribution of an optical system.

As pointed out in Table 1, and in Fig. 1, for the Barker sequence of length $L = 5$ and $L = 13$, the autocorrelation function has several positive sidelobes. Consequently, from Eq. (12) we note that the modulation of the sinusoidal variations will have a positive sign. And therefore, at the Gaussian image $W = 0$, the irradiance distribution has a maximum value.

Furthermore, it is interesting to recognize that from the viewpoint of modular arithmetic [21], the lengths $L = 5$ and $L = 13$ are both congruent to unity modulo four. That is $\mathrm{Mod}_4\,(5) = \mathrm{Mod}_4\,(13) = 1$. Their explicit, Strehl ratios versus focus errors are the following. For $L = 5$,

$$S_5(W) = \left(\frac{1}{9} \right) \left[5 + 2\ \cos\left(2\,\pi \left(\frac{2}{5\,\lambda} \right) W \right) + 2\ \cos\left(2\,\pi \left(\frac{4}{5\,\lambda} \right) W \right) \right]\ \operatorname{sinc}^2\left(\frac{W}{5\,\lambda} \right). \tag{15}$$

And for $L = 13$,

$$S_{13}(W) = \left(\frac{1}{25} \right) \left[\begin{array}{l} 13 + 2\ \cos\left(2\,\pi \left(\frac{2}{13\,\lambda} \right) W \right) + 2\ \cos\left(2\,\pi \left(\frac{4}{13\,\lambda} \right) W \right) + \\ +2\ \cos\left(2\,\pi \left(\frac{6}{13\,\lambda} \right) W \right) + 2\ \cos\left(2\,\pi \left(\frac{8}{13\,\lambda} \right) W \right) + \\ +2\ \cos\left(2\,\pi \left(\frac{10}{13\,\lambda} \right) W \right) + 2\ \cos\left(2\,\pi \left(\frac{12}{13\,\lambda} \right) W \right) \end{array} \right] \operatorname{sinc}^2\left(\frac{W}{13\,\lambda} \right). \tag{16}$$

On the other hand, for the Barker sequence of length $L = 3$, $L = 7$, and $L = 11$, the autocorrelation function has negative sidelobes; as was indicated in Table 1. Consequently, from Eq. (12) we claim that the modulation of the sinusoidal variations has a negative sign. And therefore, at the Gaussian image $W = 0$, the irradiance distribution has minimum value.

It is also interesting to note that from the viewpoint of modular arithmetic, the lengths $L = 3$, $L = 7$, and $L = 11$ are congruent to three modulo four. That is $\mathrm{Mod}_4\,(3) = \mathrm{Mod}_4\,(7) = \mathrm{Mod}_4$

Optics EXPRESS

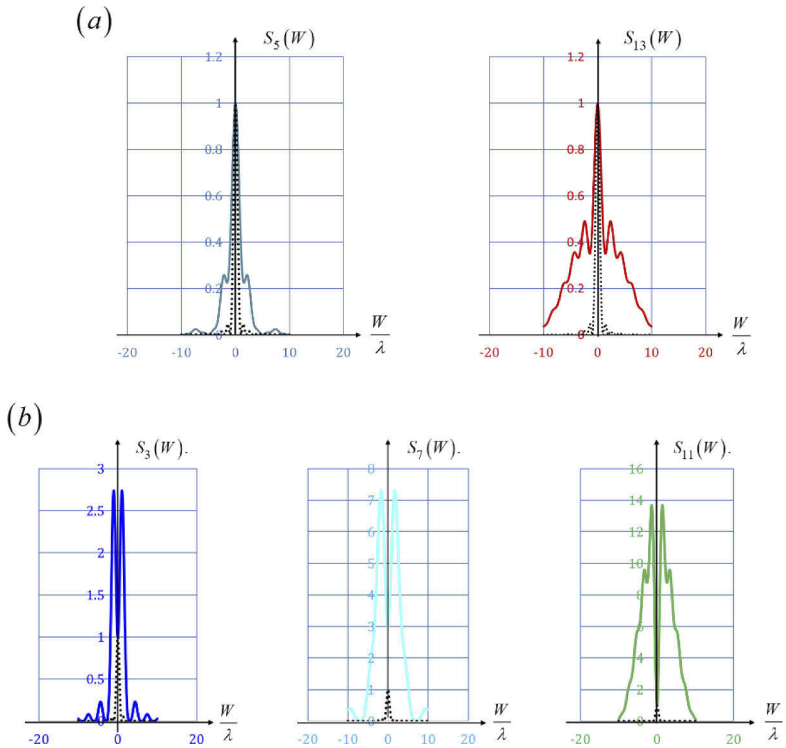

Fig. 5. Axial irradiance distributions associated to the use of the Barker rings. In (a) the mask is coded with the Barker sequences of length 5 and 13, respectively. In (b) the mask is coded with the Barker sequences of length 3, 7 and 11, respectively. The dotted curve, in black, is the axial irradiance of a clear pupil aperture.

(11) = 3. Their explicit, Strehl ratios versus focus errors are the following. For L = 3,

$$S_3(W) = \left[3 - 2\ \cos\left(2\,\pi\left(\frac{2}{3\,\lambda}\right)W\right)\right]\ \mathrm{sinc}^2\left(\frac{W}{3\,\lambda}\right). \tag{17}$$

For L = 7,

$$S_7(W) = \left[\begin{array}{c} 7 - 2\ \cos\left(2\,\pi\left(\frac{2}{7\,\lambda}\right)W\right) \\ -2\ \cos\left(2\,\pi\left(\frac{4}{7\,\lambda}\right)W\right) - 2\ \cos\left(2\,\pi\left(\frac{6}{7\,\lambda}\right)W\right) \end{array}\right]\ \mathrm{sinc}^2\left(\frac{W}{7\,\lambda}\right). \tag{18}$$

And for L = 11,

$$S_{11}(W) = \left[\begin{array}{c} 11 - 2\ \cos\left(2\,\pi\left(\frac{2}{11\,\lambda}\right)W\right) - 2\ \cos\left(2\,\pi\left(\frac{4}{11\,\lambda}\right)W\right) \\ -2\ \cos\left(2\,\pi\left(\frac{6}{11\,\lambda}\right)W\right) - 2\ \cos\left(2\,\pi\left(\frac{8}{11\,\lambda}\right)W\right) \\ -2\ \cos\left(2\,\pi\left(\frac{8}{11\,\lambda}\right)W\right) \end{array}\right]\ \mathrm{sinc}^2\left(\frac{W}{11\,\lambda}\right). \tag{19}$$

The five above axial irradiance distributions indicate clearly that one can extend the axial irradiance distribution, by employing concentric rings, which are coded with the Barker sequences.

5. Summarizing comments

For extending the focal depth of an optical system, we have described an optical method that employs a transparent mask, which is composed by a set of concentric disks. Equivalently, we have discussed the use of a spatial filter that broadens the axial impulse response, and in this manner, the mask increases the Strehl ratio versus focus errors.

For designing the proposed mask, we have described a procedure for generating a set of L partitions on 1-D pupil aperture. At each partition, the complex amplitude transmittance is equal to one value of a Barker sequence of length L. As a second step, on the optical design of the mask, we have discussed a geometrical transformation that maps the 1-D partitions into a set of concentric disks.

Then, we have obtained a mathematical formulation that describes the influence of the proposed disks on the figure of merit known as the Strehl ratio versus focus errors. Out of our mathematical formulation, we have shown that the axial irradiance distributions are composed by two terms. The first term is an axial uniform background. And the second term contains several sinusoidal variations. The modulation of the sinusoidal variations was related to the autocorrelation of the Barker sequences.

We have reported five new expressions, which indicate that the irradiance distributions are spread, without zero values, along the optical axis. Related graphs depict the spreading of the axial irradiance distributions.

For potential imaging applications, we have noted that at the focal plane the axial irradiance distribution can have a maximum value, if the Barker lengths are $L = 5$ and $L = 13$. These two lengths are congruent to unity modulo four.

On the other hand, for optical trapping, it is convenient to have an axial irradiance distribution a minimum value, at the focal plane. This optical characteristic can be if the set of concentric disks are coded with the Barker sequences of length $L = 3$, $L = 5$ and $L = 11$. From the viewpoint of modular arithmetic, these lengths are congruent to three modulo four.

Acknowledgements. We express our sincere gratitude to the reviewers for their thorough criticism as well as for their valuable suggestions.

Disclosures. The authors declare that there are no conflicts of interest related to this article. However, we would like to indicate that a reduced, preliminary version of the current results have been submitted as contribution to honor Prof. De, founder of the Optical Society of India.

Data availability. Data underlying the results presented in this paper are not publicly available at this time but may be obtained from the authors upon reasonable request.

References

1. R. D. Swift, R. B. Wattson, J. A. Decker Jr., R. Paganetti, and M. Harwit, "Hadamard transform imager and imaging spectrometer," Appl. Opt. **15**(6), 1595–1609 (1976).
2. M. Harwit and N. J. A. Sloane, *Hadamard Transform Optics* (Academic Press, 1979).
3. L. N. Hazra and A. Banerjee, "Application of Walsh function in generation of optimum apodizers," J. Opt. **5**(1), 19–26 (1976).
4. L. N. Hazra, "A new class of optimum amplitude filters," Opt. Commun. **21**(2), 232–236 (1977).
5. M. De and L. N. Hazra, "Real time image restoration through Walsh filtering," Opt. Acta **24**(3), 211–220 (1977).
6. L. N. Hazra, P. K. Purkait, and M. De, "Apodization of aberrated pupils," Can. J. Phys. **57**(9), 1340–1346 (1979).
7. L. N. Hazra and A. Guha, "Far field diffraction properties of radial Walsh filters," J. Opt. Soc. Am. A **3**(6), 843–846 (1986).
8. L. N. Hazra, "Walsh filters in tailoring of resolution in microscopic imaging," Micron **38**(2), 129–135 (2007).
9. Jorge Ojeda-Castañeda, J. E. A. Landgrave, and C. M. Gómez-Sarabia, "The use of conjugate phase plate in the analysis of the frequency response of optical systems designed for extended depth of field," Appl. Opt. **47**(22), E99–E105 (2008).
10. Jorge Ojeda-Castaneda and Cristina M. Gómez-Sarabia, "Tuning field depth at high resolution by pupil engineering," Adv. Opt. Photon. **7**(4), 814–880 (2015).
11. Cristina M. Gómez-Sarabia, Luis Ledesma-Carrillo, and Jorge Ojeda-Castañeda, "Reducing field depth: annular Hadamard masks," Appl. Opt. **59**(22), 6632–6637 (2020).
12. Jorge Ojeda-Castañeda, M. Martínez-Corral, and P. Andrés, "Zero axial irradiance by annular screens with angular variation," Appl. Opt. **31**(22), 4600–4602 (1992).
13. Jorge Ojeda-Castañeda and Gustavo Ramírez, "Zone plates for zero axial irradiance," Opt. Lett. **18**(2), 87–89 (1993).
14. Adolf W. Lohmann, Jorge Ojeda-Castañeda, and Gustavo Ramírez, "Zone Plates encoding Limaçonal Variations," Opt. Commun. **114**(1-2), 30–36 (1995).

Optics EXPRESS

15. Cristina M. Gómez-Sarabia, Luis M. Ledesma-Carrillo, Cipriano Guzmán-Cano, Miguel Torres-Cisneros, Rafael Guzmán-Cabrera, and Jorge Ojeda-Castañeda, "Pseudo-random masks for angular alignment," Appl. Opt. **56**(28), 7869–7876 (2017).
16. Jorge Ojeda-Castaneda and L. R. Berriel-Valdos, "Zone plate for arbitrarily high focal depth," Appl. Opt. **29**(7), 994–997 (1990).
17. Sucharita Sanyal and Ajay Ghosh, "High focal depth with a quasi-bifocus birefringent lens," Appl. Opt. **39**(14), 2321–2325 (2000).
18. Haifeng Wang and Fuxi Gan, "High focal depth with a pure-phase apodizer," Appl. Opt. **40**(31), 5658–5662 (2001).
19. Haifeng Wang and Fuxi Gan, "Phase-shifting apodizers for increasing focal depth," Appl. Opt. **41**(25), 5263–5266 (2002).
20. R. H. Barker, "Group synchronizing of binary digital systems," in *Communication Theory* (Butterworth, 1953) pp. 273–287.
21. R. A. Beaumont and R. S. Pierce, *The algebraic foundations of mathematics* (Addison-Wesley, 1963) pp. 175–188.
22. Athanasios Papoulis, *Systems and transforms with applications in optics* (McGraw-Hill, 1968) p. 329.
23. Joseph W. Goodman, *Introduction to Fourier optic* (McGraw-Hill, 1968) p. 67.